NANO LETTERS

Letter

pubs.acs.org/NanoLett

Directionally-Controlled Periodic Collimated Beams of Surface Plasmon Polaritons on Metal Film in Ag Nanowire/Al_2O_3/Ag Film Composite Structure

Hong Wei,* Xiaorui Tian, Deng Pan, Li Chen, Zhili Jia, and Hongxing Xu*

Institute of Physics, Chinese Academy of Sciences, and Beijing National Laboratory for Condensed Matter Physics, Beijing 100190, China

Supporting Information

ABSTRACT: Plasmonics holds promise for the realization of miniaturized photonic devices and circuits in which light can be confined and controlled at the nanoscale using surface plasmon polaritons (SPPs), surface waves of collective oscillations of electrons at a metal/dielectric interface. However, realizing plasmonic applications fundamentally requires the ability to guide and transfer SPPs in different plasmonic structures. Here the generation and control of periodic collimated SPP-beams are reported in composite structures of silver nanowire on silver film with a dielectric spacer layer between them. It is revealed that the collimated beams on the silver film originate from the interference between film-SPPs generated by two SPP modes on the nanowire. The direction of the collimated beams can be readily tuned by changing the thickness of the dielectric spacer. These findings demonstrate the transfer of nanowire SPPs to film SPPs and offer a new approach to generate nondiffracting SPP-beams, which could facilitate the design and development of complex plasmonic systems for device applications and enable the tailoring of SPP radiation and SPP−matter interactions.

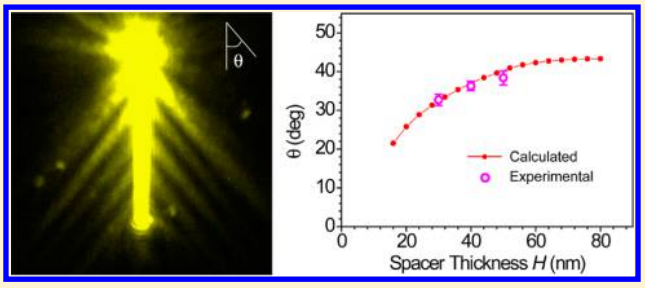

KEYWORDS: *Surface plasmons, collimated beams, Ag nanowire/Al_2O_3/Ag film composite structure, waveguide, interference*

Surface plasmons in metal nanostructures are attractive because they enable the confinement of electromagnetic fields to nanometer length scales and can be used to manipulate light and light−matter interactions.[1−3] The extremely strong confinement of the electromagnetic field in the nanogap between neighbored metal nanopaprticles can allow surface-enhanced Raman spectroscopy with single molecule sensitivity and the generation of white-light supercontinuum and deep-UV light.[4−7] Surface plasmons also enable the miniaturization of nanophotonic devices and circuits beyond the diffraction limit. Plasmonics is thus regarded as one of the promising solutions for the integration of photonics and electronics at nanoscale dimensions for tomorrow's sensing and information technology.[8−10] Among various plasmon-based nanophotonic devices, nanowaveguide is one of the most important components for building the plasmonic circuitry. Metal film and one-dimensional (1D) plasmonic waveguide are two fundamental structures supporting propagating surface plasmon polaritons (SPPs).[1]

Metal film provides a platform to build and integrate functional components for nanophotonic applications. For example, semiconductor nanowires on metal film with a thin dielectric spacing layer have been demonstrated as plasmonic nanolasers.[11−13] Moreover, this kind of composite structure can be used as hybrid plasmonic waveguide for long distance SPP guiding and loss compensation.[14−16] The SPPs on metal film suffer spatial spread during propagation due to the diffraction effect. Thus, bare metal film can hardly be used for controllable and directional SPP guiding. Recently, it was demonstrated that the SPPs on metal film can be diffraction-free as plasmonic Airy beam and cosine-Gauss beam that are launched by drilling grating structures on the metal film.[17−22] One-dimensional plasmonic waveguides with well-defined geometrical structures can support SPPs to enable the confinement and guiding of light at subwavelength dimensions.[3] A number of 1D waveguide structures have been proposed and investigated, for example, metal nanowires (NWs),[23−38] metal stripes,[39−41] and nanogrooves in metal film.[42,43] Integrating metal film with 1D nanowaveguides can facilitate the development of plasmon-based nanophotonic circuits. Moreover, to be able to integrate plasmonic building blocks in functional devices requires mechanistic insight into the processes governing the transmission of SPPs between different plasmonic structures and guidance on how these processes could be efficiently controlled.

In this Letter, we report the generation and control of periodic collimated beams of SPPs in composite structure of Ag NW/Al_2O_3/Ag film. It is revealed that the collimated beams on the metal film originate from interference between film-SPPs

Received: October 20, 2014
Revised: December 12, 2014
Published: December 16, 2014

dx.doi.org/10.1021/nl504018q | *Nano Lett.* 2015, 15, 560−564

emanating from different SPP modes on the NW. The direction and the period of these collimated beams are determined by the wave vectors of the NW SPP modes. By changing the thickness of the Al_2O_3 spacer, the direction of the collimated SPP beams can be readily tuned. Our research here not only provides a novel way to generate nondiffracting SPP-beams on metal film surface but also demonstrates the conversion of NW SPPs to collimated film-SPPs. As both NW and metal film are important waveguides supporting SPPs, their combination and SPP transfer between them are favorable for the on-chip integration of nanophotonic circuits.

The cross section of the composite structure we studied is schematically shown in Figure 1a. The sample consists of a 120 nm thick Ag film deposited on a glass substrate, a dielectric layer of Al_2O_3, and chemically synthesized Ag NWs that were subsequently dropped onto the Al_2O_3 layer surface. An additional Al_2O_3 layer of 30 nm thickness was then deposited on top of the NWs. Finally, to be able to visualize the SPP propagation in the NW-film samples we spin-coated CdSe/ZnS core/shell quantum dots (QDs) onto the sample surface.[44] Figure 1b shows the scanning electron microscopy (SEM) image of a Ag NW on Al_2O_3 coated Ag film. When laser light of 633 nm wavelength was shone onto one end of the NW (top in Figure 1c), SPPs were excited and propagated to the other end of the NW, where a clear signal of the SPP-to-light output was observed (bottom end of the NW in Figure 1c). Because the SPPs excite the QDs on the sample surface to fluoresce with an intensity that is proportional to the electromagnetic near-field intensity, we can, by imaging the QD fluorescence in our NW-film samples, obtain the near-field intensity distribution thereon.[44−46]

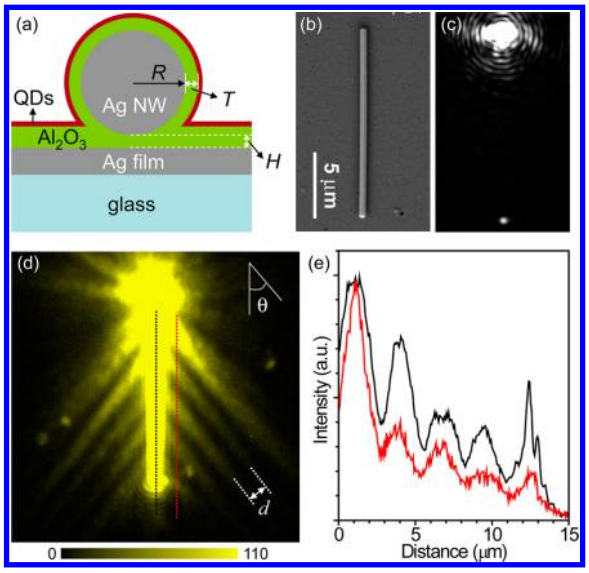

Figure 1. (a) Schematic cross section of the sample. (b) SEM image of a Ag NW/Al_2O_3/Ag film sample with R = 200 nm, H = 40 nm, and T = 30 nm. (c) Optical image of the sample with laser light of 633 nm wavelength focused on the top end of the NW. (d) QD fluorescence from the sample that is excited by laser light focused on the top end of the NW. The angle relative to the NW θ and the period of the collimated SPP beams d are indicated. (e) Intensity profiles of QD fluorescence measured along the marker lines in panel d. The black and red curves are normalized with the maximum intensity.

From the QD-fluorescence imaging it is clearly seen that not only the QDs on the NW but many QDs across a large portion of the sample surrounding the NW are excited (Figure 1d). Two characteristic features can be discerned from the QD-fluorescence imaging. First, we observe a longitudinal, periodic modulation (with a period of approximately 2.7 μm) of the near-field distribution along the NW (see the QD fluorescence intensity profile recorded along the black marker line in Figure 1d and shown in Figure 1e, as well as Figure S1, Supporting Information). This longitudinal modulation along the NW results from interference between different SPP modes on the NW.[47,48] As expected, the intensity decreases further away from the excitation point due to Ohmic and radiative losses. The second, and, for this Letter, main observation is that collimated beams of SPPs emanate periodically from both sides of the NW and propagate on the film surface for several microns along straight lines formed at an angle with respect to the NW (Figure 1d). The periodicity of these collimated beams along the direction parallel to the NW (red dotted line in Figure 1d and red curve in Figure 1e) is identical to the periodicity of the on-wire SPP longitudinal modulation (black dotted line in Figure 1d and black curve in Figure 1e). The angle θ between these beams and the NW is about 38°, and the period d is about 1.6 μm.

To understand the origin of these collimated SPP beams, we performed finite-element-method simulations using the commercial multiphysics software package COMSOL. To allow comparison with the experiment, we used in the simulation the same values for the Ag NW radius (R), the top Al_2O_3 coating thickness (T), and the thickness of Al_2O_3 spacer between the Ag NW and the Ag film (H) as in the experiment for Figure 1. Furthermore, we excited the SPPs in the simulations in a way similar to the experiments by illuminating one end of the wire with a focused Gaussian beam (Figure 2a). Refractive indexes of n = 1.62 for Al_2O_3 and n = 0.05625 + 4.276i for Ag[49] were used in the simulations. Because in the experiments the near-field intensity probed by QDs via their emitted fluorescence is proportional to the intensity of electric field $|E|^2$ on the top Al_2O_3 surface, our simulations of the $|E|$ distribution in the NW-film give the same information about the SPP propagation in this system as in the experiments.

The simulations clearly reproduce the electric field intensity profiles seen in the experiments. In particular, they reproduce the collimated beams of SPPs emanating from the NW and onto the Ag film (Figure 2b,c) as seen in the experiment (Figure 1d). Moreover, both the distance between adjacent beams emanating from the NW and the angle with respect to the NW as obtained by the simulations are very close to the experimentally observed values. Analyses of the top- and side-views of the simulated electric field profiles reveal that the collimated film SPPs emanate from the side-antinodes in the periodic modulation of the near-field intensity along the NW (Figure 2b and top panel in Figure 2c). This is further corroborated by analysis of the cross-sectional images taken at positions corresponding to antinodes and nodes in the intensity distribution at the top of the NW (white dashed lines i and ii in the top panel of Figure 2c, and corresponding cross-sectional images in the bottom panel in the same figure).

To gain deeper insight into the origin of the observed collimated SPP beams on the film, we used the mode analysis module in COMSOL multiphysics software to analyze the SPP modes in the studied Ag NW/Al_2O_3/Ag film system. Because of the electromagnetic coupling between the Ag NW and film, the SPP modes in the composite structure are different to those on NWs that are surrounded by a homogeneous dielectric

dx.doi.org/10.1021/nl504018q | Nano Lett. 2015, 15, 560−564

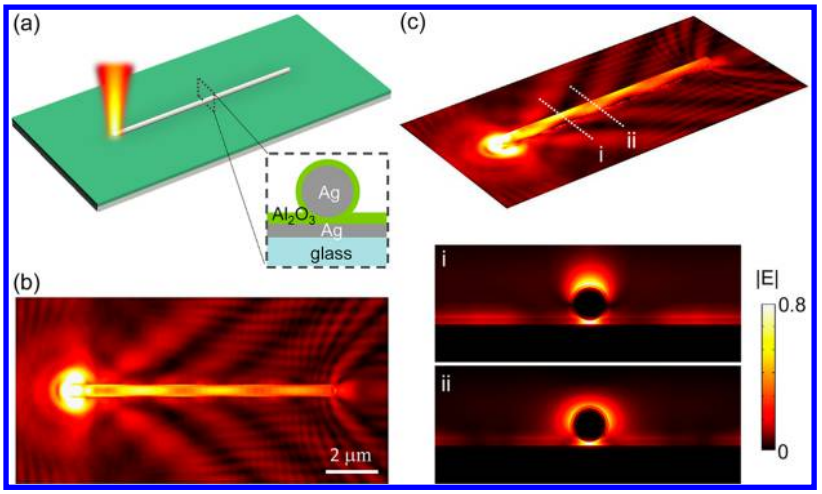

Figure 2. (a) Sketch of the simulation setup. (b) Top-view of the simulated electric field $|E|$ distribution at the surface of the top Al_2O_3 layer. (c) Tilted view of the result shown in panel b (top panel), and two cross-sectional images (bottom panel) of the simulated $|E|$ distribution along the white dashed lines in the top panel. The parameters in the simulations are R = 200 nm, H = 40 nm, and T = 30 nm. The incident light in the simulations is polarized parallel to the NW and has a wavelength of 632.8 nm.

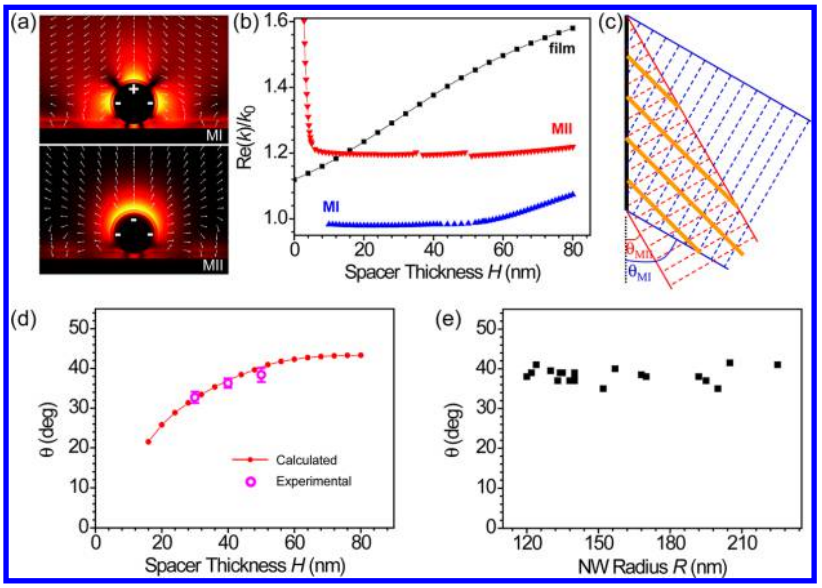

Figure 3. (a) Simulated electric field distributions of the two leaky SPP modes on the NW. Surface charges are schematically drawn. The sample parameters in the simulations are R = 200 nm, H = 40 nm, T = 30 nm, and Ag film thickness 120 nm. The wavelength is 632.8 nm. (b) Simulated real parts of the wave vectors Re(k) of the two SPP modes on the NW, as well as the SPPs on the film, as a function of the spacer thickness H. The k_0 is the wave vector of the excitation light. Blue, red, and black curves correspond to mode MI, MII, and film-SPPs, respectively. The values for R, T, Ag film thickness, and wavelength are the same as those in panel a. (c) Schematic drawing for the mechanism of generating collimated SPP beams. The black line represents the NW. The blue and red dashed lines represent the wavefronts of the SPP waves launched by modes MI and MII on NW, respectively. The orange lines depict the collimated beams formed due to constructive interference between the two SPP waves. (d) Calculated and experimental values of the propagation angles of collimated SPP beams as a function of spacer thickness. The calculated results were obtained using data in panel b. The experimental data are mean values with standard deviation as the error. The experimental data are from eight NWs for H = 30 and 40 nm, and from 20 NWs for H = 50 nm. The NW radii in the experimental measurements were in the range 120 < R < 225 nm. (e) Experimentally measured angles of collimated beams as a function of NW radius for H = 50 nm.

environment.[47] The electric field distributions of two leaky modes (named MI and MII) are shown in Figure 3a (see Supporting Information for another leaky mode excited by polarization perpendicular to the NW, and the simulation results for Ag NW with pentagonal cross section). These two modes are weakly confined and radiate to the silver film. The coherent superposition of these two modes results in the field distributions on the NW as shown by the cross-sectional images in Figure 2c, which indicates that the collimated SPP-beams on the film are resulted from these two modes. We further analyzed the real parts of the wave vectors of these two SPP modes (hereafter denoted Re(k_{MI}) and Re(k_{MII})) and that of the SPPs on the film (hereafter denoted Re(k_F)), and simulated their dependence on the spacer thickness H (Figure 3b). We found that Re(k_F) increases monotonically with increased spacer layer thickness. In contrast, Re(k_{MII}) first decreases sharply with increased spacer thickness and crosses the Re(k_F) curve at $H \approx$ 13.8 nm. However, Re(k_{MI}) is always smaller than Re(k_F) (as well as Re(k_{MII})). When Re(k) of a NW-SPP mode becomes smaller than Re(k_F), the SPPs on the NW start

dx.doi.org/10.1021/nl504018q | Nano Lett. 2015, 15, 560−564

radiating into the Ag film. Here the MII mode radiates to the film when $H > 13.8$ nm, while the MI mode is radiative for any spacer thickness.

Armed with the insight obtained from the analysis of Re(k) of the SPP modes on the NW and film, we can now understand the origin of the collimated beams of SPPs observed in our Ag NW/Al_2O_3/Ag film system. The two NW-SPP modes MI and MII generate two SPP waves on the Ag film propagating along different directions (schematically shown by the blue and red lines in Figure 3c), which are determined by the ratio between the wave vectors of the SPPs on the NW and on the film, according to the phase matching condition $\cos \theta_M = \mathrm{Re}(k_{NW})/\mathrm{Re}(k_F)$, where $\mathrm{Re}(k_{NW})$ is the real part of the wave vector of the SPP mode on the NW, and θ_M is the angle between the NW and the propagation direction of film SPPs generated by a certain NW-SPP mode. For the film SPPs generated by MI and MII modes, the propagation direction can be determined by $\cos \theta_{MI} = \mathrm{Re}(k_{MI})/\mathrm{Re}(k_F)$ and $\cos \theta_{MII} = \mathrm{Re}(k_{MII})/\mathrm{Re}(k_F)$, respectively.

The periodically modulated nondiffracting SPP beams observed in our experiments and simulations are then generated on the film because of interference between these two film-SPP waves related to the MI and MII modes. The direction of the collimated beams is along the symmetry axis of the intersecting angle of the two SPP waves on the film. The generation and directionality of these collimated beams are illustrated in Figure 3c where the blue and red dashed lines represent the wavefronts of the two SPP waves on the film. The constructive interference of the two SPP waves leads to the collimated beams on the two sides of the NW. The angle of the collimated beams (orange lines in Figure 3c) relative to the NW is $\theta = (\theta_{MI} + \theta_{MII})/2$.

Using the data in Figure 3b, we calculate the angle of the collimated beams of SPPs relative to the NW axis. The calculation results show that the propagation angle θ of the collimated beams increases with increasing Al_2O_3 thickness (Figure 3d). Moreover, the simulated angles show an excellent agreement with the experimental values (Figure 3d). While the angle of collimated beams strongly depends on the spacer layer thickness, our experimental results show that it only weakly depends on the NW radius (Figure 3e).

The periodicity of the collimated SPP beams on the film is directly related to the intersecting angle of two film-SPP waves and can be readily obtained from the beating period Λ of the two modes on the NW, i.e., period of collimated beams

$$d = \Lambda \sin \theta = \lambda \sin \theta/(\mathrm{Re}(k_{MII})/k_0 - \mathrm{Re}(k_{MI})/k_0)$$

where λ is the wavelength of the excitation light, which is 633 nm here, and k_0 is the wave vector of the excitation light. By using the data in Figure 3b, we can obtain $d = 1.8$ μm for a NW-film structure with the spacer thickness $H = 40$ nm, which agrees well with the experimentally measured value in Figure 1. The distance that the collimated beams propagate non-dispersively is determined by the overlapping area of the two film-SPP waves. If the NW length is 14 μm (the same as the NW in Figure 1), the calculated longest nondiffracting distance (the third collimated beam from the top as drawn in Figure 3c) is 27.6 μm. The length of the experimentally observed collimated beams is limited by the SPP damping.

Our observation is not only of fundamental but also technological interest. Understanding how to generate, transfer, and guide SPPs in different plasmonic structures is crucial for the realization of plasmonics-based applications. The mechanism behind the observed collimated SPP beams provides a simple and versatile tool to rationally design and control the generation and propagation of SPP beams. By managing the wave vector of the SPPs, their radiation properties can be rationally tailored. Therefore, collimated propagation and radiation in plasmonic structures can be potentially integrated into nanophotonic networks. As a first proof-of-principle we have investigated collimated SPP generation in coupled Ag NW-nanoparticle structure on top of Al_2O_3 coated Ag film (Figure 4a). The QD fluorescence image in Figure 4b shows

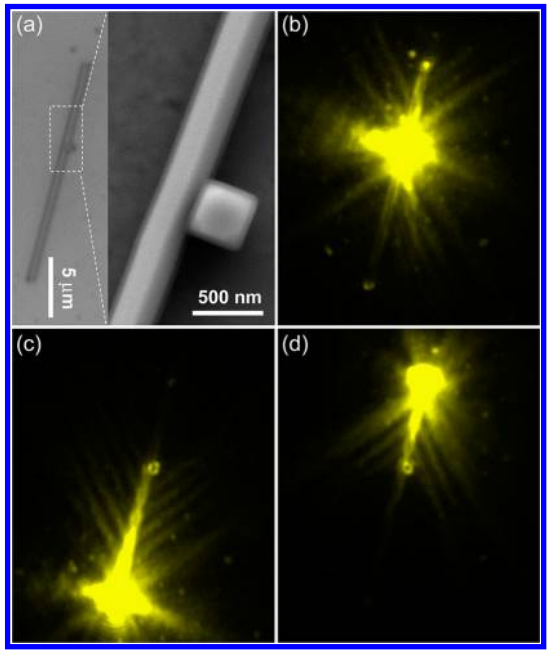

Figure 4. (a) Optical image (left) and SEM image (right). (b–d) QD fluorescence images for excitation at the wire–particle junction (b), at the bottom end of the NW (c), and at the top end of the NW (d). The radius of the NW is about 138 nm, spacer thickness $H = 50$ nm.

that SPPs excited at the nanoparticle position propagate nondiffractingly on the Ag film in opposite directions. By focusing the excitation light on the bottom or top end of the NW, the collimated SPPs can be launched with different propagation directions (Figure 4c,d). These collimated branches could be used as virtual waveguides to transfer electromagnetic energy to other parts in a network. The controllable SPP transmission between different plasmonic structures by SPP–SPP transfer may benefit the plasmonic integrations for functional nanophotonic devices. The interference of SPPs provides flexibility in manipulating light at the nanometer scale and developing all-optical plasmonic components for circuitry applications.[50]

In conclusion, in the composite structure of Ag NW/Al_2O_3/Ag film, we show that periodic collimated SPP beams on the film can be generated by exciting the NW SPPs. The collimated beams originate from the interference between film-SPPs emanating from two SPP modes on the NW. The propagation direction of the collimated SPP beams can be simply controlled by tuning the thickness of the spacer layer between the Ag NW and the Ag film. These findings offer a new approach to generate nondiffracting SPP beams, which may be used for optical interconnects. Moreover, the composite structure of metal NW and metal film enables the combination of NW-SPPs and film-SPPs and provides a platform to integrate functional

dx.doi.org/10.1021/nl504018q | Nano Lett. 2015, 15, 560–564

nanophotonic/nanoelectronic components based on metal NWs or films, which may facilitate the development of plasmonic devices and on-chip integration of nanophotonic circuits.

■ ASSOCIATED CONTENT

Supporting Information

Experimental methods, additional figure of QD fluorescence, another leaky mode excited by perpendicular polarization, and simulation results for Ag NW with pentagonal cross section. This material is available free of charge via the Internet at http://pubs.acs.org.

■ AUTHOR INFORMATION

Corresponding Authors

*E-mail: weihong@iphy.ac.cn.
*E-mail: hxxu@iphy.ac.cn.

Notes

The authors declare no competing financial interest.

■ ACKNOWLEDGMENTS

This work was supported by the Ministry of Science and Technology of China (Grant No. 2012YQ12006005), the National Natural Science Foundation of China (Grant Nos. 11134013, 11227407, and 11374012), the "Knowledge Innovation Project" (Grant No. KJCX2-EW-W04), and the "Strategic Priority Research Program (B)" (Grant No. XDB07030100) of Chinese Academy of Sciences (CAS). The authors thank the Laboratory of Microfabrication in the Institute of Physics, CAS, for experimental support.

■ REFERENCES

(1) Barnes, W. L.; Dereux, A.; Ebbesen, T. W. *Nature* **2003**, *424*, 824−830.
(2) Schuller, J. A.; Barnard, E. S.; Cai, W. S.; Jun, Y. C.; White, J. S.; Brongersma, M. L. *Nat. Mater.* **2010**, *9*, 193−204.
(3) Gramotnev, D. K.; Bozhevolnyi, S. I. *Nat. Photonics* **2010**, *4*, 83−91.
(4) Xu, H. X.; Bjerneld, E. J.; Kall, M.; Borjesson, L. *Phys. Rev. Lett.* **1999**, *83*, 4357−4360.
(5) Xu, H. X.; Aizpurua, J.; Kall, M.; Apell, P. *Phys. Rev. E* **2000**, *62*, 4318−4324.
(6) Muhlschlegel, P.; Eisler, H. J.; Martin, O. J. F.; Hecht, B.; Pohl, D. W. *Science* **2005**, *308*, 1607−1609.
(7) Kim, S.; Jin, J. H.; Kim, Y. J.; Park, I. Y.; Kim, Y.; Kim, S. W. *Nature* **2008**, *453*, 757−760.
(8) Tong, L. M.; Wei, H.; Zhang, S. P.; Xu, H. X. *Sensors* **2014**, *14*, 7959−7973.
(9) Ozbay, E. *Science* **2006**, *311*, 189−193.
(10) Wei, H.; Wang, Z. X.; Tian, X. R.; Kall, M.; Xu, H. X. *Nat. Commun.* **2011**, *2*, 387.
(11) Oulton, R. F.; Sorger, V. J.; Zentgraf, T.; Ma, R. M.; Gladden, C.; Dai, L.; Bartal, G.; Zhang, X. *Nature* **2009**, *461*, 629−632.
(12) Lu, Y. J.; Kim, J.; Chen, H. Y.; Wu, C. H.; Dabidian, N.; Sanders, C. E.; Wang, C. Y.; Lu, M. Y.; Li, B. H.; Qiu, X. G.; Chang, W. H.; Chen, L. J.; Shvets, G.; Shih, C. K.; Gwo, S. *Science* **2012**, *337*, 450−453.
(13) Liu, X. F.; Zhang, Q.; Yip, J. N.; Xiong, Q. H.; Sum, T. C. *Nano Lett.* **2013**, *13*, 5336−5343.
(14) Oulton, R. F.; Sorger, V. J.; Genov, D. A.; Pile, D. F. P.; Zhang, X. *Nat. Photonics* **2008**, *2*, 496−500.
(15) Liu, N.; Wei, H.; Li, J.; Wang, Z. X.; Tian, X. R.; Pan, A. L.; Xu, H. X. *Sci. Rep.* **2013**, *3*, 1967.
(16) Alam, M. Z.; Aitchison, J. S.; Mojahedi, M. *Laser Photon. Rev.* **2014**, *8*, 394−408.
(17) Salandrino, A.; Christodoulides, D. N. *Opt. Lett.* **2010**, *35*, 2082−2084.
(18) Zhang, P.; Wang, S.; Liu, Y. M.; Yin, X. B.; Lu, C. G.; Chen, Z. G.; Zhang, X. *Opt. Lett.* **2011**, *36*, 3191−3193.
(19) Minovich, A.; Klein, A. E.; Janunts, N.; Pertsch, T.; Neshev, D. N.; Kivshar, Y. S. *Phys. Rev. Lett.* **2011**, *107*, 116802.
(20) Li, L.; Li, T.; Wang, S. M.; Zhang, C.; Zhu, S. N. *Phys. Rev. Lett.* **2011**, *107*, 126804.
(21) Lin, J.; Dellinger, J.; Genevet, P.; Cluzel, B.; de Fornel, F.; Capasso, F. *Phys. Rev. Lett.* **2012**, *109*, 093904.
(22) Li, L.; Li, T.; Wang, S. M.; Zhu, S. N. *Phys. Rev. Lett.* **2013**, *110*, 046807.
(23) Dickson, R. M.; Lyon, L. A. *J. Phys. Chem. B* **2000**, *104*, 6095−6098.
(24) Ditlbacher, H.; Hohenau, A.; Wagner, D.; Kreibig, U.; Rogers, M.; Hofer, F.; Aussenegg, F. R.; Krenn, J. R. *Phys. Rev. Lett.* **2005**, *95*, 257403.
(25) Sanders, A. W.; Routenberg, D. A.; Wiley, B. J.; Xia, Y. N.; Dufresne, E. R.; Reed, M. A. *Nano Lett.* **2006**, *6*, 1822−1826.
(26) Knight, M. W.; Grady, N. K.; Bardhan, R.; Hao, F.; Nordlander, P.; Halas, N. J. *Nano Lett.* **2007**, *7*, 2346−2350.
(27) Akimov, A. V.; Mukherjee, A.; Yu, C. L.; Chang, D. E.; Zibrov, A. S.; Hemmer, P. R.; Park, H.; Lukin, M. D. *Nature* **2007**, *450*, 402−406.
(28) Allione, M.; Temnov, V. V.; Fedutik, Y.; Woggon, U.; Artemyev, M. V. *Nano Lett.* **2008**, *8*, 31−35.
(29) Fang, Y. R.; Wei, H.; Hao, F.; Nordlander, P.; Xu, H. X. *Nano Lett.* **2009**, *9*, 2049−2053.
(30) Li, Z. P.; Hao, F.; Huang, Y. Z.; Fang, Y. R.; Nordlander, P.; Xu, H. X. *Nano Lett.* **2009**, *9*, 4383−4386.
(31) Song, M. X.; Bouhelier, A.; Bramant, P.; Sharma, J.; Dujardin, E.; Zhang, D. G.; Colas-des-Francs, G. *ACS Nano* **2011**, *5*, 5874−5880.
(32) Shegai, T.; Miljkovic, V. D.; Bao, K.; Xu, H. X.; Nordlander, P.; Johansson, P.; Kall, M. *Nano Lett.* **2011**, *11*, 706−711.
(33) Fang, Z. Y.; Fan, L. R.; Lin, C. F.; Zhang, D.; Meixner, A. J.; Zhu, X. *Nano Lett.* **2011**, *11*, 1676−1680.
(34) Rewitz, C.; Keitzl, T.; Tuchscherer, P.; Huang, J.; Geisler, P.; Razinskas, G.; Hecht, B.; Brixner, T. *Nano Lett.* **2012**, *12*, 45−49.
(35) Wei, H.; Xu, H. X. *Nanophotonics* **2012**, *1*, 155−169.
(36) Guo, X.; Ma, Y. G.; Wang, Y. P.; Tong, L. M. *Laser Photon. Rev.* **2013**, *7*, 855−881.
(37) Hu, Q.; Xu, D. H.; Zhou, Y.; Peng, R. W.; Fan, R. H.; Fang, N. X.; Wang, Q. J.; Huang, X. R.; Wang, M. *Sci. Rep.* **2013**, *3*, 3095.
(38) Pan, D.; Wei, H.; Jia, Z. L.; Xu, H. X. *Sci. Rep.* **2014**, *4*, 4993.
(39) Weeber, J. C.; Krenn, J. R.; Dereux, A.; Lamprecht, B.; Lacroute, Y.; Goudonnet, J. P. *Phys. Rev. B* **2001**, *64*, 045411.
(40) Zia, R.; Schuller, J. A.; Brongersma, M. L. *Phys. Rev. B* **2006**, *74*, 165415.
(41) Anderson, L. J. E.; Zhen, Y. R.; Payne, C. M.; Nordlander, P.; Hafner, J. H. *Nano Lett.* **2013**, *13*, 6256−6261.
(42) Pile, D. F. P.; Gramotnev, D. K. *Opt. Lett.* **2004**, *29*, 1069−1071.
(43) Bozhevolnyi, S. I.; Volkov, V. S.; Devaux, E.; Laluet, J. Y.; Ebbesen, T. W. *Nature* **2006**, *440*, 508−511.
(44) Wei, H.; Li, Z. P.; Tian, X. R.; Wang, Z. X.; Cong, F. Z.; Liu, N.; Zhang, S. P.; Nordlander, P.; Halas, N. J.; Xu, H. X. *Nano Lett.* **2011**, *11*, 471−475.
(45) Wei, H.; Ratchford, D.; Li, X. Q.; Xu, H. X.; Shih, C. K. *Nano Lett.* **2009**, *9*, 4168−4171.
(46) Ditlbacher, H.; Krenn, J. R.; Felidj, N.; Lamprecht, B.; Schider, G.; Salerno, M.; Leitner, A.; Aussenegg, F. R. *Appl. Phys. Lett.* **2002**, *80*, 404−406.
(47) Zhang, S. P.; Wei, H.; Bao, K.; Hakanson, U.; Halas, N. J.; Nordlander, P.; Xu, H. X. *Phys. Rev. Lett.* **2011**, *107*, 096801.
(48) Wei, H.; Zhang, S. P.; Tian, X. R.; Xu, H. X. *Proc. Natl. Acad. Sci. U.S.A.* **2013**, *110*, 4494−4499.
(49) Johnson, P. B.; Christy, R. W. *Phys. Rev. B* **1972**, *6*, 4370−4379.
(50) Bao, Y. J.; Peng, R. W.; Shu, D. J.; Wang, M.; Lu, X.; Shao, J.; Lu, W.; Ming, N. B. *Phys. Rev. Lett.* **2008**, *101*, 087401.